

Functional connectome reorganization after pontine stroke is associated with better motor outcomes

March 4, 2021

Emily Olafson, Keith Jamison, Hesheng Liu, Danhong Wang, Joel Bruss, Aaron Boes, Amy Kuceyeski

Introduction

Motor deficits are the most common and disruptive symptoms of ischemic stroke, but spontaneous recovery of motor function occurs for most patients [1]. This motor recovery is dependent on the ability of brain networks to functionally reorganize and compensate for lost brain areas [2]. As demonstrated by animal models, the functional role of motor regions damaged by stroke may be adopted by surviving tissue around the site of the lesion, but brain areas distant to the damaged tissue with similar function and connectivity as the lesion site have also been shown to compensate for lost function in animals, typically when the initial infarct is large [3, 4, 5, 6].

In humans, functional reorganization underlying post-stroke motor recovery has been studied with resting-state functional magnetic resonance imaging (fMRI). Strong evidence suggests that crucial to eventual motor recovery is the restoration of interhemispheric resting-state functional connectivity (FC) between the primary motor cortices [7, 8, 9], but less is known about how the brain's functional networks change on a greater spatial and temporal scale after stroke. Altered network topology [10] and recruitment of other networks aside from the motor network such as the frontoparietal network [11, 12] have been implicated in the recovery process, but network changes at a high temporal resolution have not been well documented.

Prior studies investigating neural correlates of motor recovery have focused almost exclusively on supratentorial strokes that impact the internal capsule and surrounding areas. Evidence suggests that for pontine strokes, which impact the connections between motor cortex and the cerebellum [13], and account for roughly 7 percent of all ischemic strokes [14] sources of motor deficits as well as recovery-related reorganization might differ from those of supratentorial strokes. Reduced blood flow as measured by arterial spin labeling has been observed in the cerebellum and cortical regions in pontine stroke [15, 16] and longitudinally, changes in cerebral blood flow in cortical areas including the supramarginal gyrus and middle occipital gyrus were related to motor recovery. Areas with abnormal blood flow over time also had abnormal FC [15], and increased degree centrality in the ipsilesional cerebellum has been related to better motor recovery [17]. The network changes associated with functional damage and subsequent recovery in pontine stroke have yet to be assessed in a longitudinal study.

Secondary damage due to diaschisis, which affects remote brain areas anatomically connected to the lesion, results in widespread disruption of functional networks [18]. Functional impairment and subsequent reorganization of areas anatomically connected to the lesion may be an important component of the recovery process that has yet to be explored. In this study, we propose a novel measure to capture adaptive functional plasticity after pontine stroke, outlined below, and connect it to patterns of structural disruption after stroke.

Connectivity to the rest of the brain is one aspect of a brain region's functional role in the network. We propose that instances of functional reorganization over time, as in the case of adjacent surviving tissue adopting the functional role of lost tissue, may be captured by identifying brain regions whose pattern of FC with the rest of the brain is more closely matched by a different brain region at a later date. Considering functional connectomes as graph, the task of identifying similar nodes (gray matter regions, in this case) between two functional connectomes can be considered a graph matching problem [19]. Graph matching has been applied recently to map individual structural connectomes to their functional connectomes [20]. Conceptually, the process of graph matching exchanges the labels of nodes when doing so results increased similarity of the two networks. When two regions exchange FC profiles, the regions are said to have been 'remapped'. We hypothesize that brain regions with more structural damage due to the lesion will more frequently functionally reorganize; that more impaired subjects will have more global functional reorganization; and that the amount of functional reorganization will correlate with the change in motor impairment between subsequent sessions.

Methods

Data description

Twenty-three first-episode stroke patients (34-74 years old; mean age 57 years; 8 female) with isolate pontine infarcts. 15 subjects had right brainstem infarcts, 9 had left brainstem infarcts (Figure 1), and is described previously [13]. Patients were scanned five times during a period of 6 months - 7, 14, 30, 90 and 180 days after stroke onset (Figure 2) on a 3T TimTrio Siemens using a 12-channel phase-array head coil. Structural images were acquired using a sagittal MP-RAGE three-dimensional T1-weighted sequence (TR, 1600ms; TE 2.15ms; flip angle, 9°, 1.0 mm isotropic voxels (FOV, 256 x 256). Each MRI session involved two to four runs (360s each run) of resting-state fMRI. Subjects were instructed to stay awake and keep their eyes open; no other task instruction was provided. Images were acquired using the gradient-echo echo-planar pulse sequence (TR, 3000ms; TE, 30ms; flip angle, 90°, 3 mm isotropic voxels).

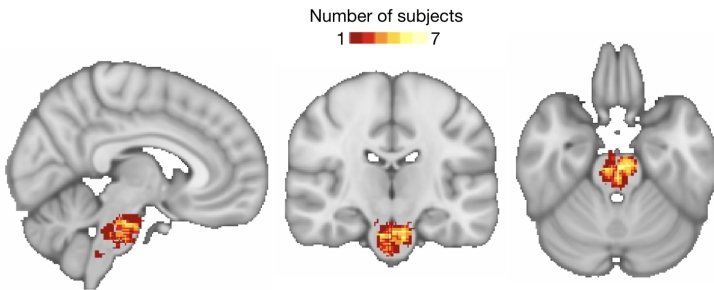


Figure 1: Distribution of lesions across the brain. Colors indicate the number of subjects with a lesion in that location.

Structural data processing

Preprocessing of the longitudinal structural data included registration of each subject's session 2-5 T1 scans to the space of session 1, collapsing co-registered files to an average, creation of a skull-stripped brain mask, followed by manual editing and binarization of the hand-edited mask. Each mask was then pushed to each of the session 2-5 T1s in native space using the inverse registration acquired from the first step. This was followed by bias field correction of the 5 T1 scans, transformation of native-space bias field-corrected data back to session 1 space, and the creation of an average bias field-corrected scan for each subject. Lesion masks were hand-drawn on these transformed T1 scans by ADB and JEB.

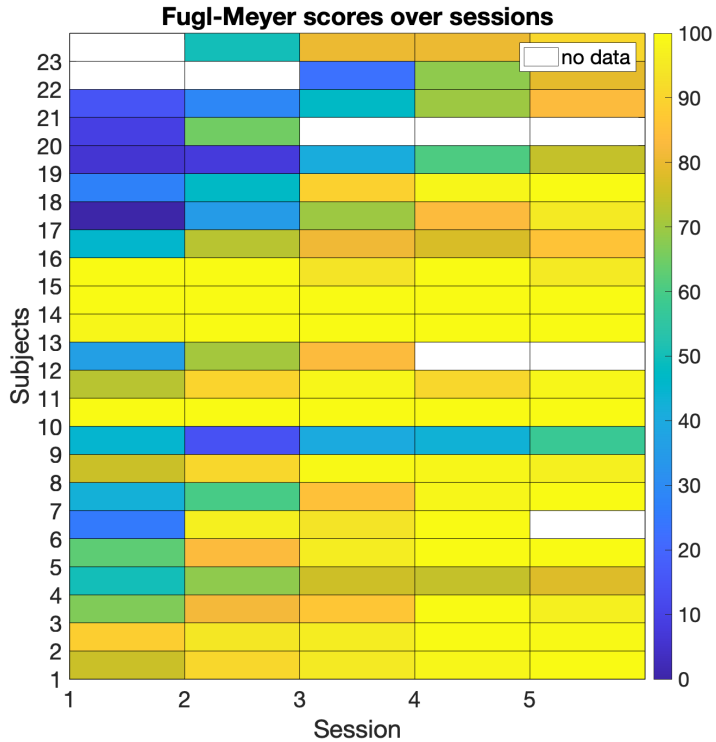


Figure 2: Fugl-Meyer scores for all subjects over sessions. Note that for subjects 6, 12, 20, 22, and 23 scores are missing. For subjects 6, 12, and 20, functional data is also missing

Functional data processing

Preprocessing of the longitudinal functional data was performed using the CONN toolbox, including functional realignment of volumes to the first volume, slice timing correction, segmentation and normalization, smoothing with a 4mm FWHM kernel, followed by a denoising protocol (comp corr) which regressed out the CSF and WM signal, as well as realignment parameters, temporal band pass filtering (0.08 - 0.9Hz). motion correction, despiking and global signal removal were also performed. Regional time series data was acquired by parcellating the scans into 268 non-overlapping brain regions using a functional atlas defined for healthy controls [21] and averaging the time course of all voxels with a region. Several analyses involve further parcellating of the 268-node atlas into 8 subnetworks [27] (Figure S2).

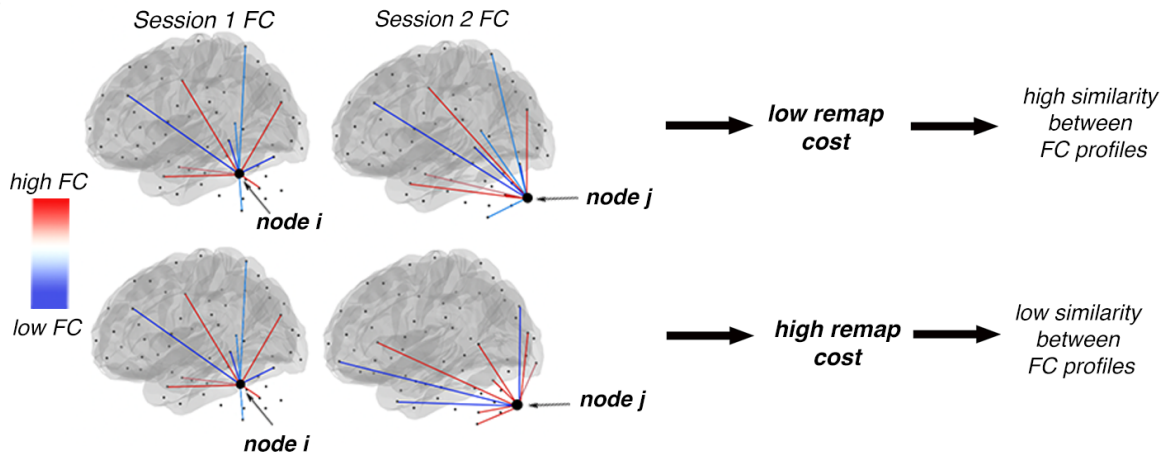
Functional connectivity calculation

Functional connectivity (FC) matrices were calculated as the regularized inverse of the precision matrix. Calculating FC using precision minimizes the effect of indirect connections and has been shown to result in FC that are more similar to structural connectivity [22, 23]. To compute the precision FC, we first took the unregularized inverse of the correlation matrix for each subject and averaged them over the sample to obtain the population-level precision matrix. We then calculated the individual's precision matrices using Tikhonov regularization, which adds a positive term to the diagonal of the precision matrix before inversion where I is the identity matrix and λ is the regularization parameter. Gamma $\gamma \in [0, 1]$ was chosen via a grid search to be the value that minimized the root mean squared error of the Frobenius norms between the regularized subject precision matrices and the population-level unregularized precision matrix, and was found to be $\gamma = 0.8$ (Supplementary Fig S1).

Estimated structural disconnection

Deficits from subcortical stroke may be related to damage at distant sites via metabolic diaschisis [24, 25]. In order to account for the impact of lesions on the structural connectome, the extent of regional structural (white matter) connectivity disruption due to the lesion was assessed for each stroke subject with the Network Modification (NeMo) Tool [26]. The Network Modification (NeMo) Tool v2 requires only an individual's lesion mask in MNI space, which was obtained as described above, to produce an estimate structural disconnection for each brain region. The newest version of the NeMo Tool, originally published in 2013, includes a reference database of connectivity networks from 420 unrelated individuals from the Human Connectome Project's (HCP) 1200 release (50 percent female, aged 25-35). The NeMo Tool begins by mapping the lesion mask into this healthy database's collection of tractography streamlines that quantify likely white matter pathways. It then identifies streamlines that pass through the lesion mask and records the gray matter regions that are at end of that streamline. Thus, the NeMo Tool produces the regional structural disconnection vector (ChaCo score, Change in Connectivity) that is an estimate of the percent of damaged streamlines terminating at each region in the atlas.

A



B

Given two **sets of nodes A, B** and a **cost function c** that determines the **cost of assigning each node in A to a corresponding node in B**, graph matching finds a one-to-one mapping function $f : A \rightarrow B$ that minimizes the sum of all the matches between A and B

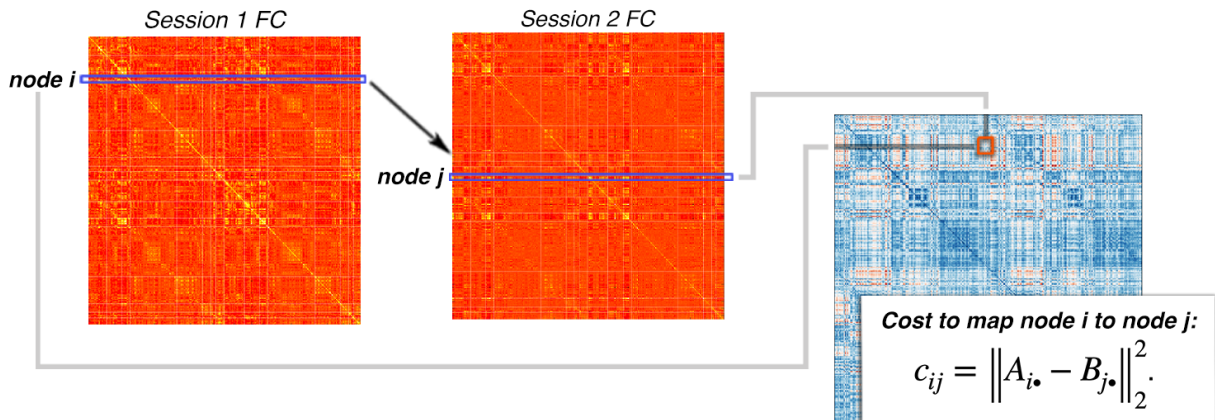


Figure 3: Graph matching procedure

Graph matching

We propose the use of graph matching to capture FC network reorganization over time; graph matching has recently been used in brain connectivity networks to map SC to FC [20]. Graph matching is an algorithmic process that maximizes the similarity between two networks by identifying a mapping between similar nodes in the two networks. One approach to identifying the optimal mapping that maximizes the similarity between two networks is with a combinatorial optimization problem known as linear assignment.

Take two $n \times n$ networks A and B and a cost function $c : A \times B \rightarrow \mathbb{R}$ that determines the cost of assigning each node in A to each node in B . Here, our cost function is the sum of the entries in the cost matrix $C = (c_{ij})$, whose entries are defined by the Euclidean distance between all pairs of rows, representing each node's FC profile, in A and B , i.e. $c_{ij} = \|A_{i\bullet} - B_{\bullet j}\|_2^2$. In this formulation, the linear assignment problem aims to construct the permutation matrix $P = (p_{ij})$ that minimizes the sum of the elements in cost matrix, i.e. $\min_P \sum_{i=1}^n \sum_{j=1}^n c_{ij} p_{ij}$. The matrix P is a permutation matrix with exactly one entry equal to 1 in each row and column, and all the rest being zero. Ones in the diagonal mean the same node in the two networks were mapped to one another, while ones in the off-diagonal indicate two different nodes were “remapped” to one another.

Here, we will use the Hungarian algorithm to solve this minimization problem and find the corresponding optimal permutation matrix. Figure 3 illustrates how the graph matching will be applied to subsequent longitudinal FC networks (from 1 week to 1 month and 1 month to 6 months) from each stroke and control individual. In the top row of Figure 3 the two brain regions (black spheres, labeled node i and node j) have very similar functional profiles, depicted with red and blue lines to other regions, and thus the cost of remapping them is low. In the second row of 3, the two brain regions have very different functional profiles and thus the cost of remapping them is high. An example cost matrix from a stroke subject's FC extracted from 1 week MRI and FC extracted from 1 month MRI is provided in (Figure S6). Unsurprisingly, the lowest costs are along the diagonal (the same region mapping to itself between time points) and across left-right homologues (in the prominent super and sub diagonals).

Estimation of functional reorganization

The permutation matrices calculated for each pair of time points for each individual were used as a measure of functional reorganization. To assess the spatial pattern of reorganization, the number of times each node was remapped across all subjects was calculated as the ‘remap frequency’, where nodes with a greater remap frequency are assigned to alternative nodes in the subsequent time point. For each subject the number nodes that were remapped can be calculated as a subject-specific measure of the extent of functional reorganization. Inspection of the patterns in the off-diagonal allows for identification of region pairs that may be remapping over time (Figure S6).

Code availability

The code for partial functional connectivity calculation, graph matching, and remap frequency is available on GitHub: <https://github.com/emilyolafson/stroke-graph-matching>

Results

Brain areas with greater structural disruption reorganize more frequently

Functional remapping frequency scores were highest in the brainstem and cerebellum, and to a lesser extent in the motor cortices (Figure 4a), similar to the spatial distribution of ChaCo (structural disconnection) scores, which were also highest in the brainstem and cerebellum (Figure S3). For each pair of longitudinal, subsequent time points, there was a significant, positive correlation between average regional ChaCo scores across subject and functional remapping frequency, indicating those regions with more baseline structural connectivity disruption also

had more remapping over time (Figure 4b). Furthermore, for about 50 percent of subjects, the nodes that remap have significantly higher ChaCo scores compared to those that do not remap (Figure S4).

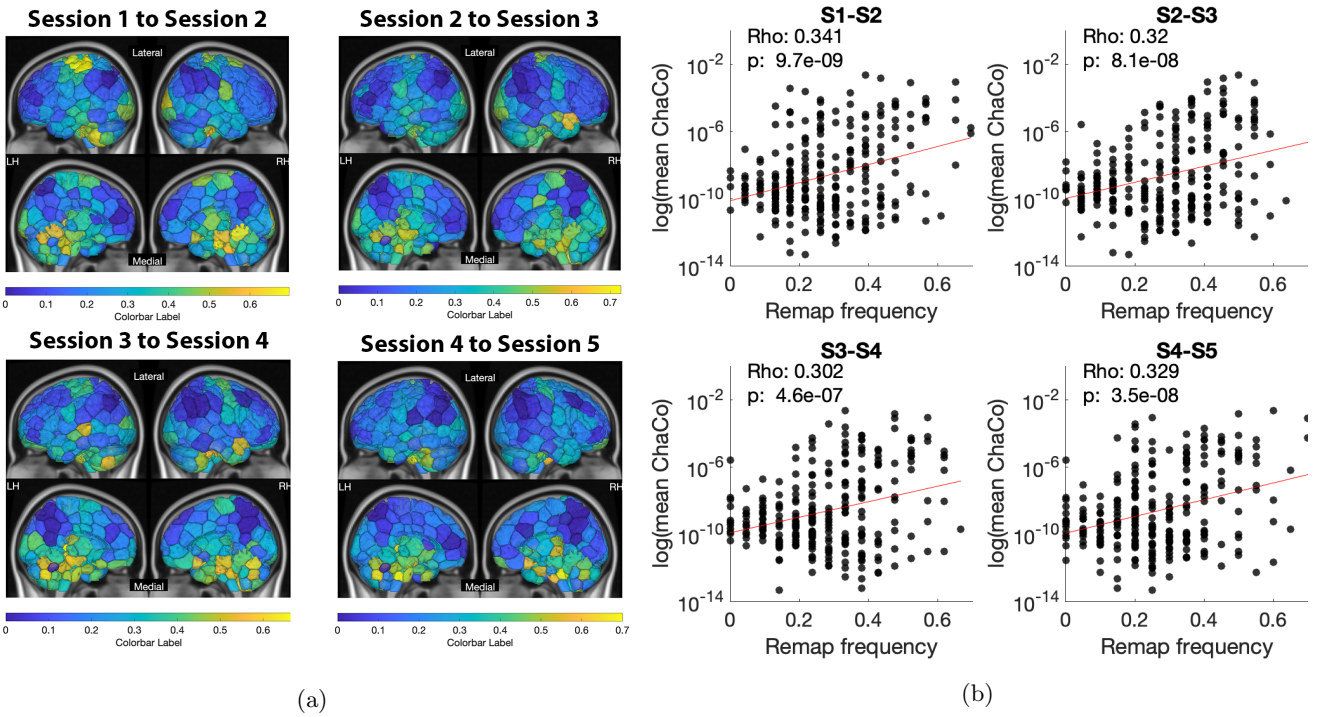


Figure 4: Remap frequencies are related to estimated structural disconnectivity. A) Node remap frequencies plotted on a glass brain for each session comparison. Inset figures display a lateral view (top row) and medial view (bottom row). B) Correlations between average ChaCo scores and node remap frequencies.

Permutation matrices

The most consistent pattern observed across subjects is that nodes are most frequently assigned to themselves (Figure S5). Nodes which do not map to themselves, which can be observed as non-zero indices in the off-diagonal of Fig S5, more frequently occur between contralateral hemispheres than within the same hemisphere. We also assessed patterns of remapping within 8 functional networks. The most remaps occur within and between nodes in the subcortical-cerebellum network, followed by the motor network, with the most remaps occurring between session 2-3 for both the subcortical-cerebellum and motor network (Figure S7).

Functional reorganization is related to impairment and recovery

We observed a significant positive correlation between baseline impairment, as measured by the Fugl-Meyer assessment at 7 days post stroke, and the number of remaps, such that patients who were more impaired at 7 days post-stroke had more remapping over the second week post-stroke (Figure 5a). The amount of recovery between subsequent sessions was positively associated with the number of remaps between sessions (Figure 5b).

Remapping in control subjects

We performed the same graph matching analysis in a separate dataset of a single individual sampled for 30 continuous days. Because of the repeated scans, 6 non-overlapping windows of both 7 days (replicating session 1 - session 2) and 14 days (replicating session 2 - session 3) were extracted (Supplementary methods).

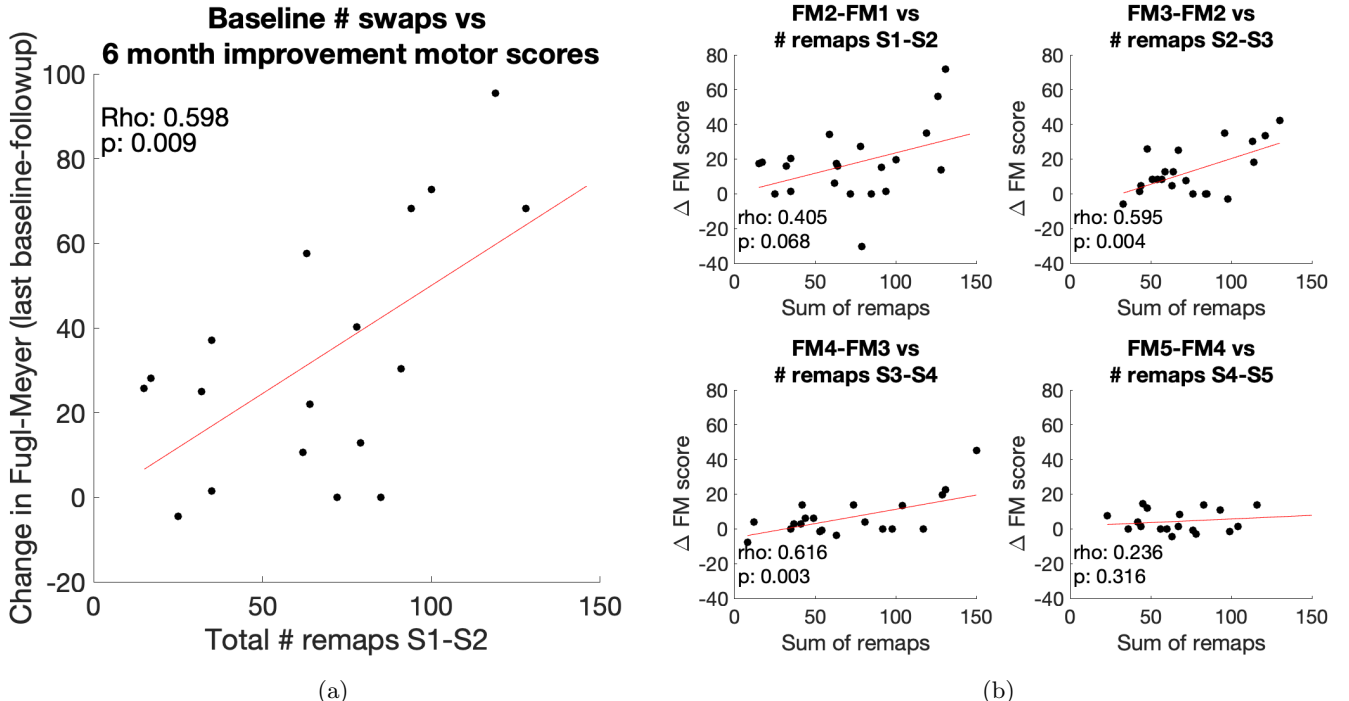


Figure 5: The amount of functional remapping between scans is related to impairment at baseline and to recovery between sessions.

Regularization produces similar results

Prior animal work suggests that functional remapping more often occurs in areas proximal to the lesion site. As such, we added a bias to the graph matching procedure that increased the cost of mapping to nodes proportional to their distance (Supplementary methods). Several β parameters were chosen based on their impact on the amount of remapping observed (Figure S10). Increasing β reduced the total number remaps, particularly the number of contralateral remaps (Figure S11) and had a similar effect across time points. The main results replicated across increasing distance bias (Figure S12, S13, S14).

Sources of noise

The impact of noise from lesions on the underlying BOLD signal is likely not driving remapping, as the maximum overlap of the lesions with each ROI is no more than 30 percent (not shown) and the average percent lesion overlap with each ROI across subjects does not correlate with remap frequency (Supplementary fig). Lesion size is also unrelated to the number of remaps for each subject (Figure S8a), but the lesion load on the corticospinal tract does significantly positively correlate with the amount of reorganization between session 1 and 2 (Figure S8b). We also found that the number of remaps was not related to motion as measured by framewise displacement (Fig S9).

Discussion

The results were consistent across increasing penalization for swaps farther apart in MNI space, despite the associated reductions in the number of swaps overall. Suggesting that remapping with more proximal nodes (specifically in the ipsilesional hemisphere) contribute to recovery and impairment

Supplementary Methods

Regularization based on distance

We replicated the analyses of the main paper after adding a regularization parameter to each node pair based on the Euclidean distance between the mean coordinates of the region in MNI space. Specifically, the Euclidean distance between two nodes i and j , in physical space, E_{ij} multiplied by a constant β was added to the cost matrix c_{ij} such that the new cost matrix equation was $c_{ij} = \|A_{i\bullet} - B_{\bullet j}\|_2^2 + \beta E_{ij}$. As such, the cost of remapping nodes that are farther apart is higher. The analysis was repeated with β parameters of 0, 1e-4, 2e-4, and 3e-4 with corresponded roughly to remap proportions of roughly 0.3, 0.10, 0.08, and 0.05, respectively.

28andMe control analysis

28andMe data [] was used due to insufficient control data. This dataset consists of a densely sampled female participant (23 y.o.) who underwent imaging for 30 consecutive days. Raw data was unavailable, but parcellated timeseries were obtained. fMRI preprocessing is detailed in [Pritshcet] and details do not deviate significantly from the processing described in this paper (same softwares used). GSR was performed on the timeseries data. Because the TR for the resting state fMRI obtained for this subject was much lower than the TR of stroke subjects (720ms vs 3000ms, respectively), the 28andMe data was downsampled to an equivalent TR. Initial scans contained 820 frames at a TR of 720ms, roughly 10 minutes of acquisition. Downsampling to keep 1 out of every 4 TRs (equivalent TR of 2880s) reduced the number of frames to 205, bringing it into the range of the stroke subjects (173-300 TRs). A stable regularized precision matrix calculation could not be performed, so the 28andMe analyses were completed using functional connectivity derived from the linear correlation between node time series.

Supplementary Figures

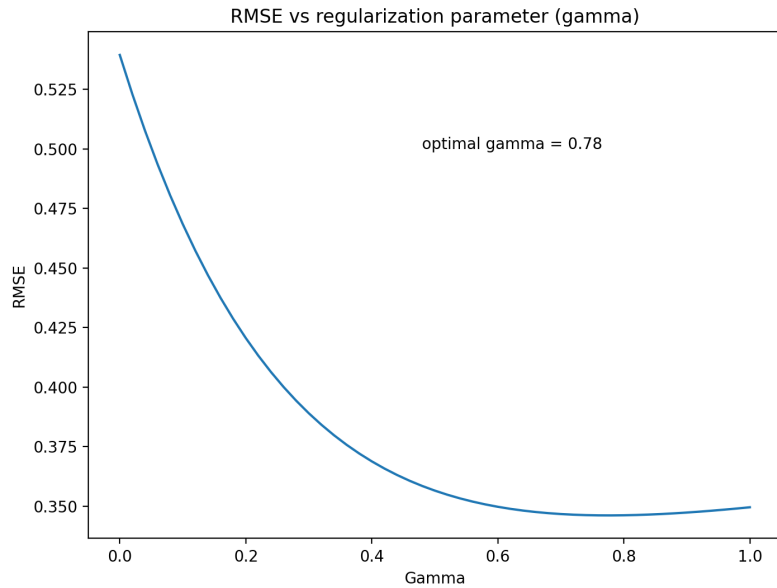


Figure S1: Results of gridsearch for gamma; plotted is the root mean squared error (RMSE) across subjects of the norm of each subject's precision matrix and the group average unregularized precision matrix at each lambda. The optimal gamma that minimized the RMSE across subjects was 0.78

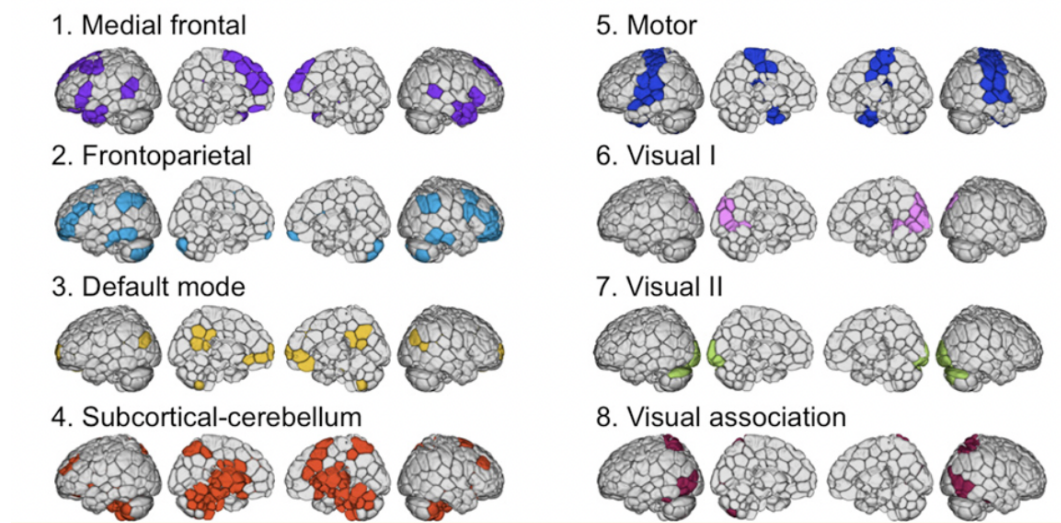


Figure S2: 8 functional networks identified by [27] by clustering healthy functional connectivity matrices.

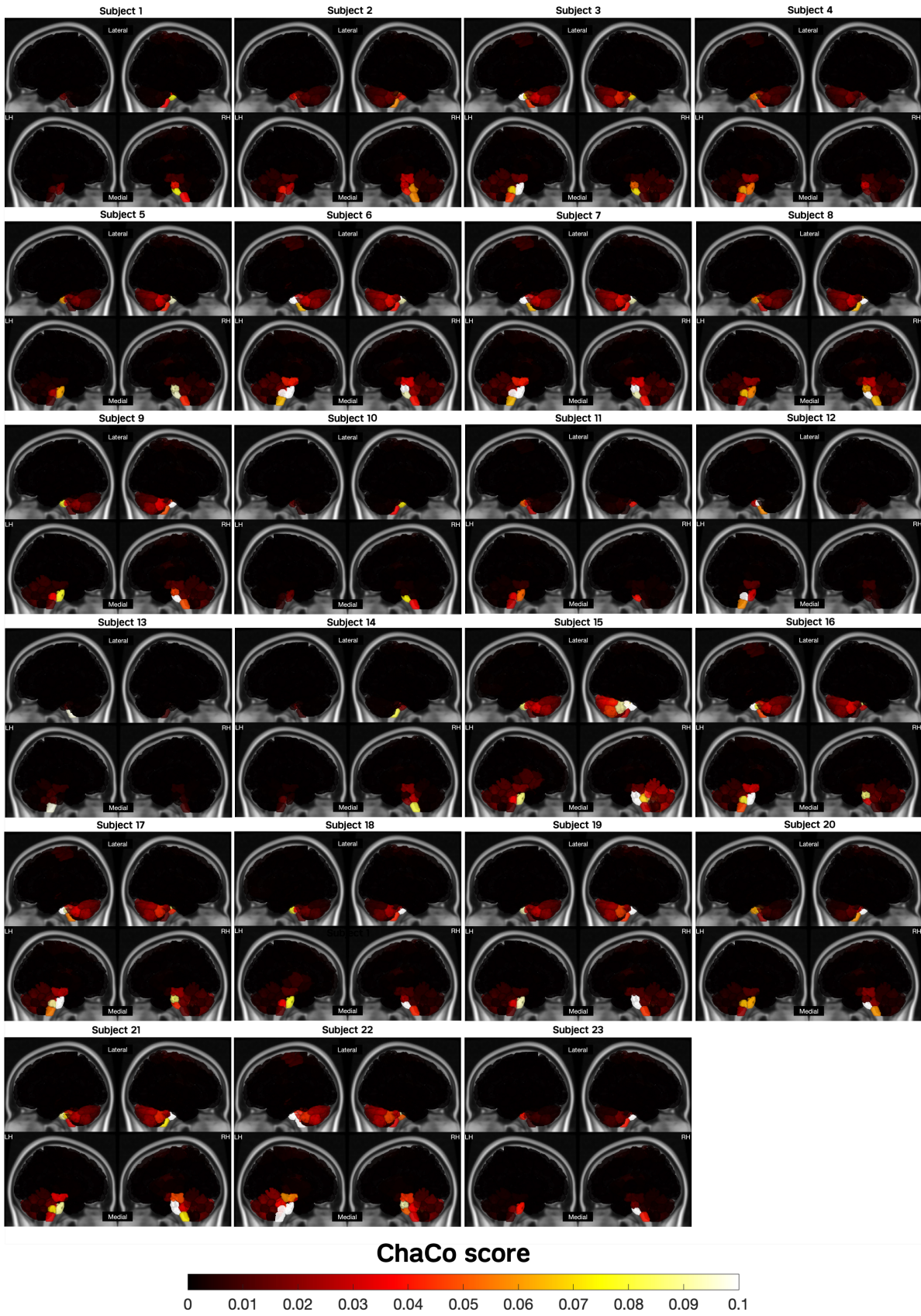


Figure S3: ChaCo scores of all subjects displayed on glass brains. Top row of each subject inset: lateral view, bottom row of each inset: medial view.

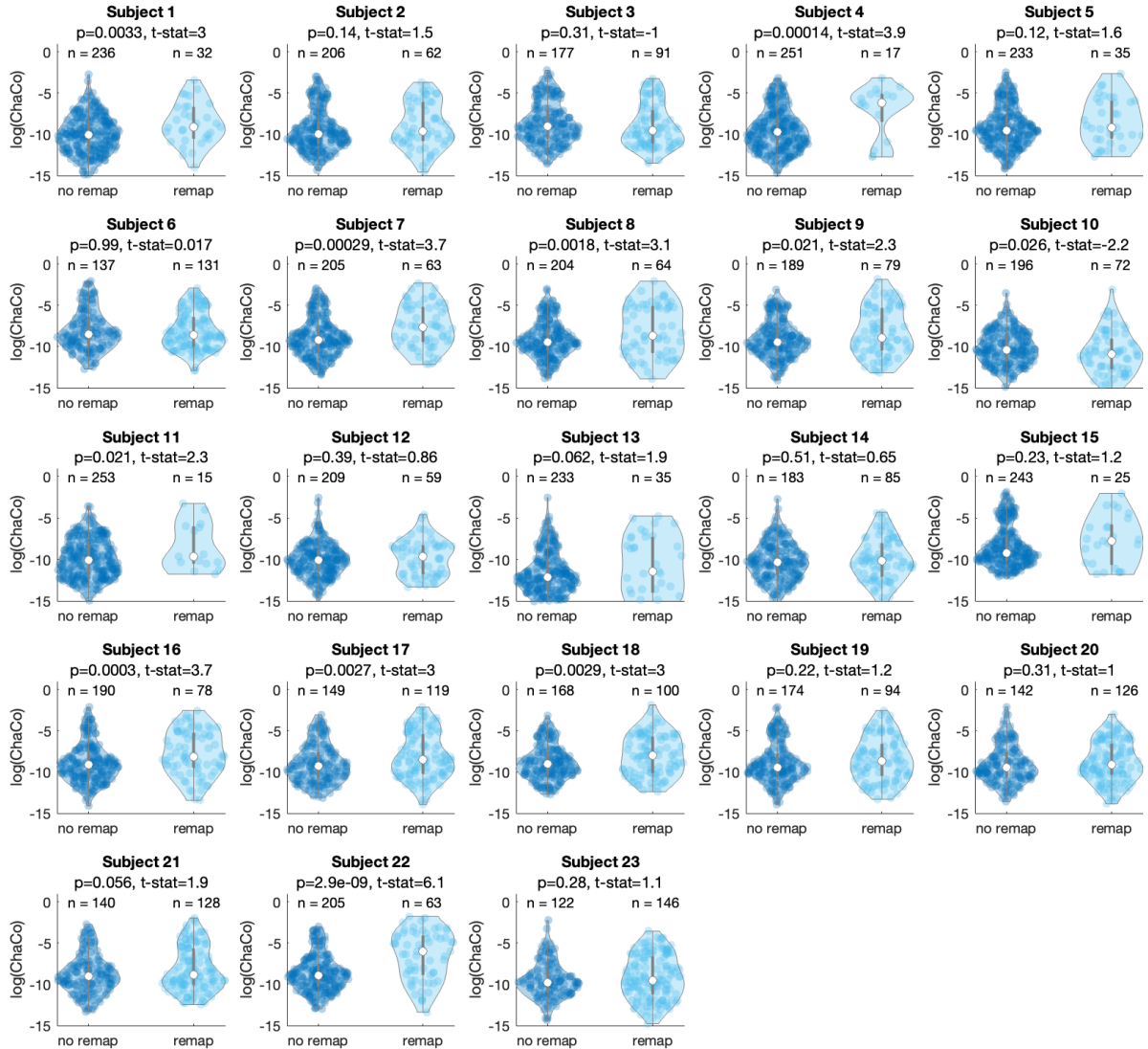


Figure S4: Paired t-tests determining whether there is a significant difference between the ChaCo scores of nodes that remap to different nodes versus those that do not. Remap patterns for the comparison between session 1 and 2 are shown; similar results are observed for other time points. No FDR correction

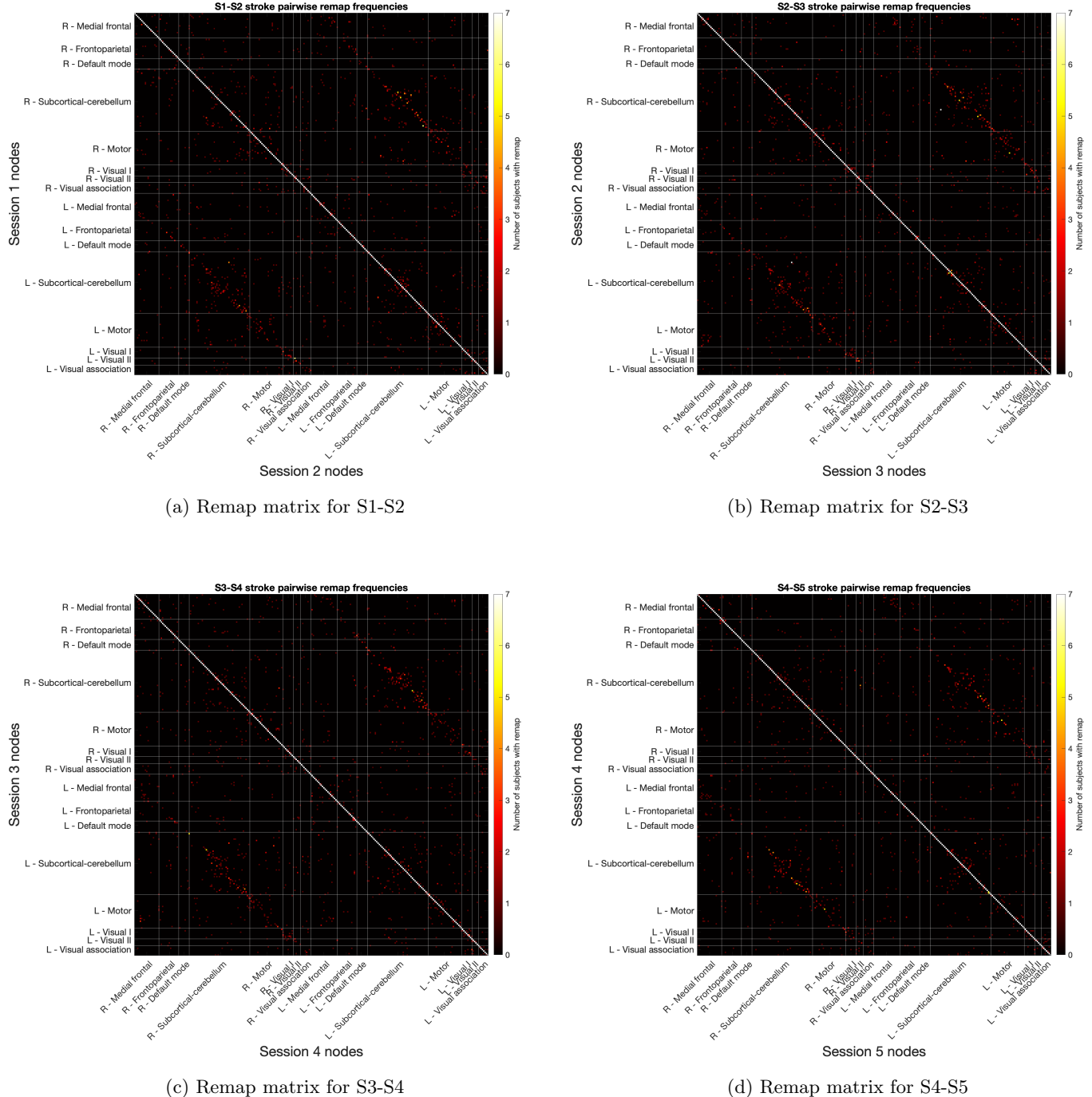


Figure S5: Permutation matrices across all 23 subjects. Each row and column represents the number of subjects where that specific remapping (node i = row i to node j = column j). The colorbar was cutoff at 7 subjects to improve visibility of off-diagonal elements.

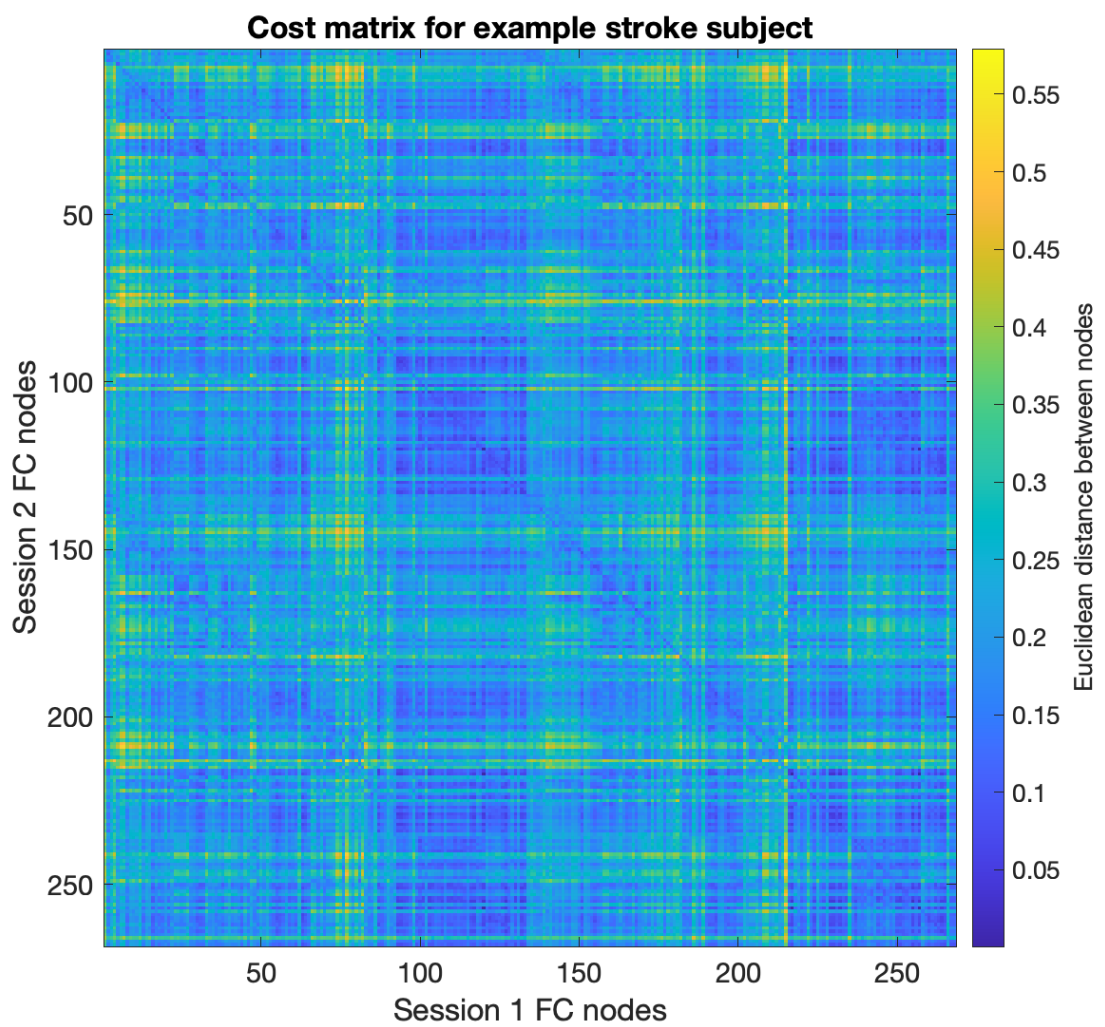


Figure S6: Cost matrix indicating the cost of remapping nodes from session 2 (vertical axis) to every other node in session 1 (horizontal axis).

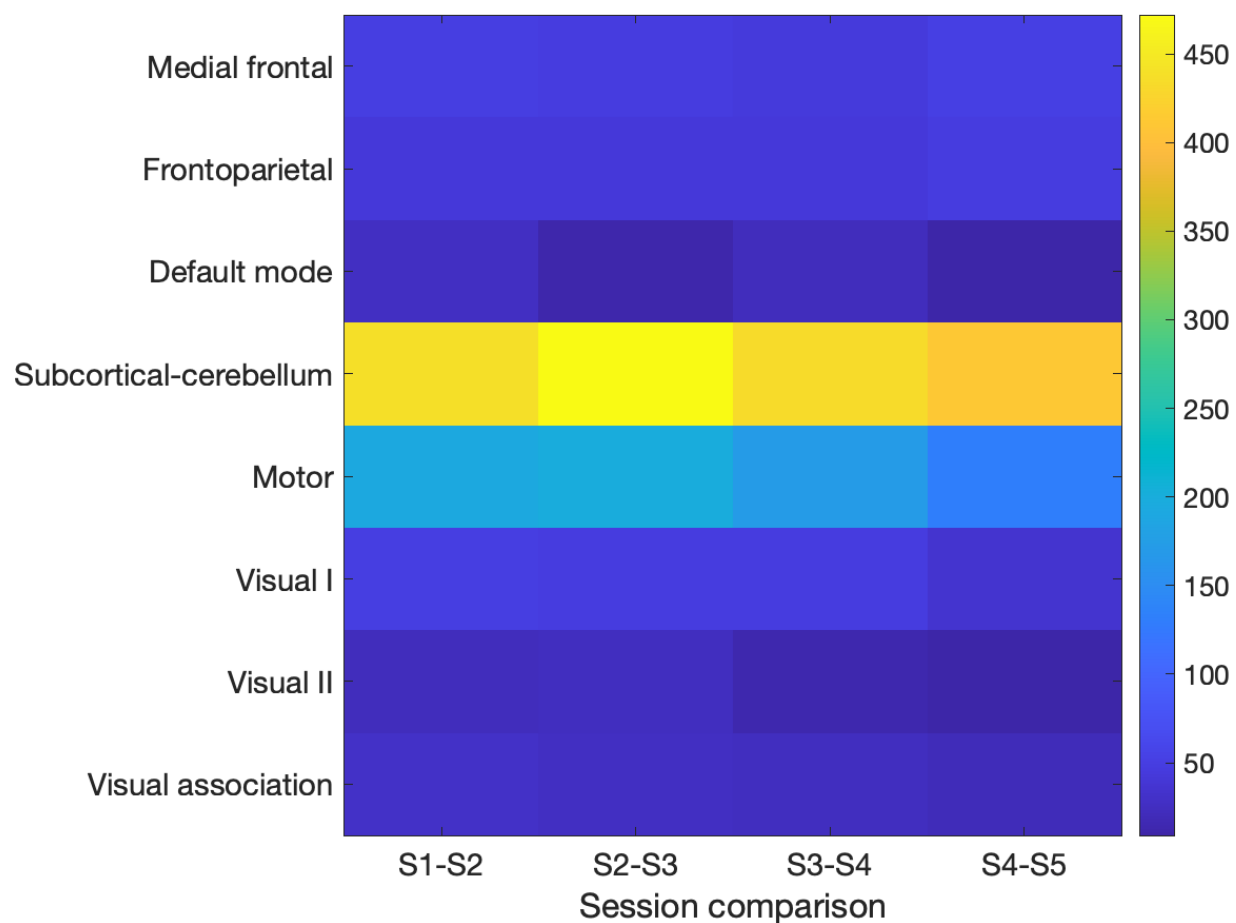


Figure S7: Sum of remaps within 8 functional networks

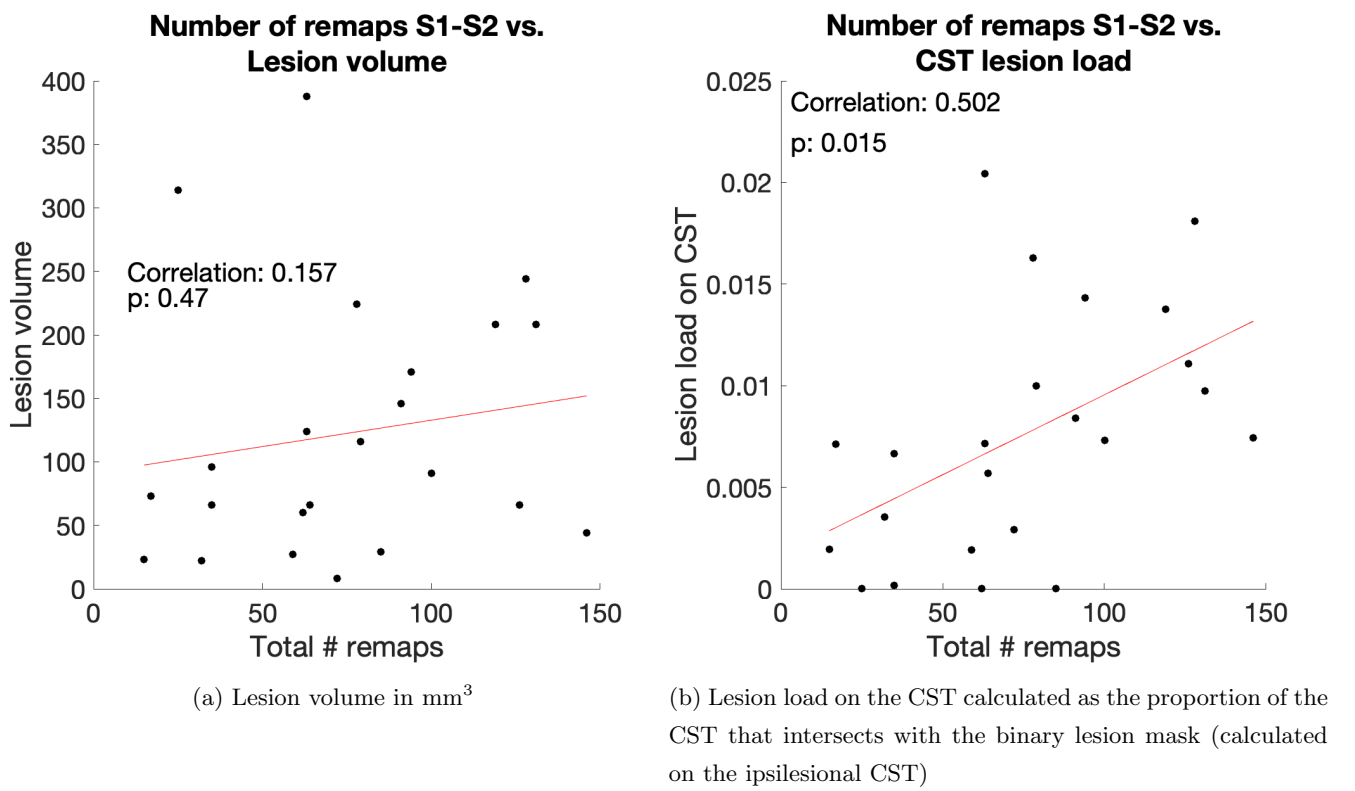


Figure S8: The extent of the lesion's impact on the ipsilesional corticospinal tract is associated with the number of remaps between session 1 and 2 whereas the total lesion volume is not.

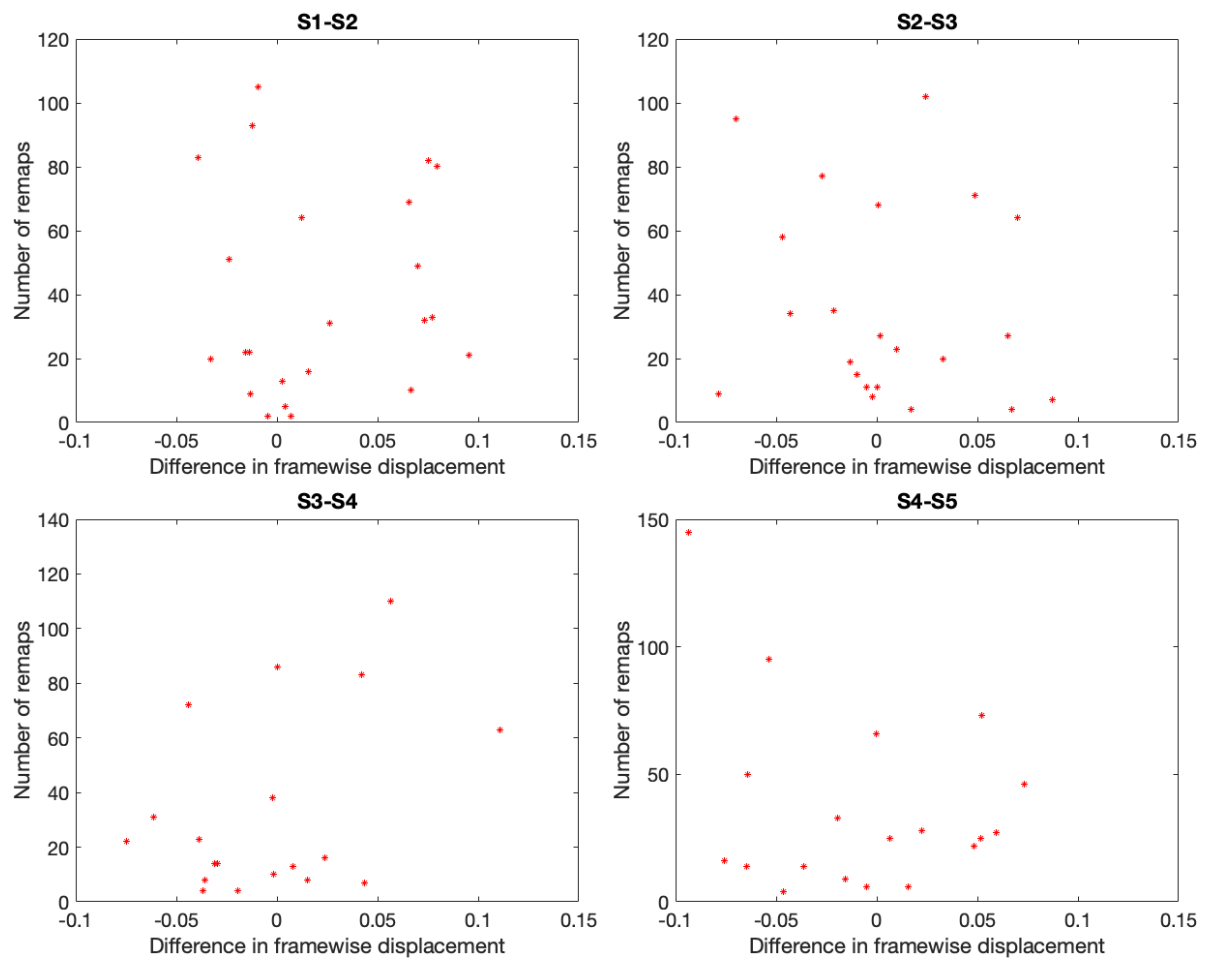


Figure S9: Correlation between difference in motion (as measured by framewise displacement) between 2 scans and the amount of remaps between the two scans.

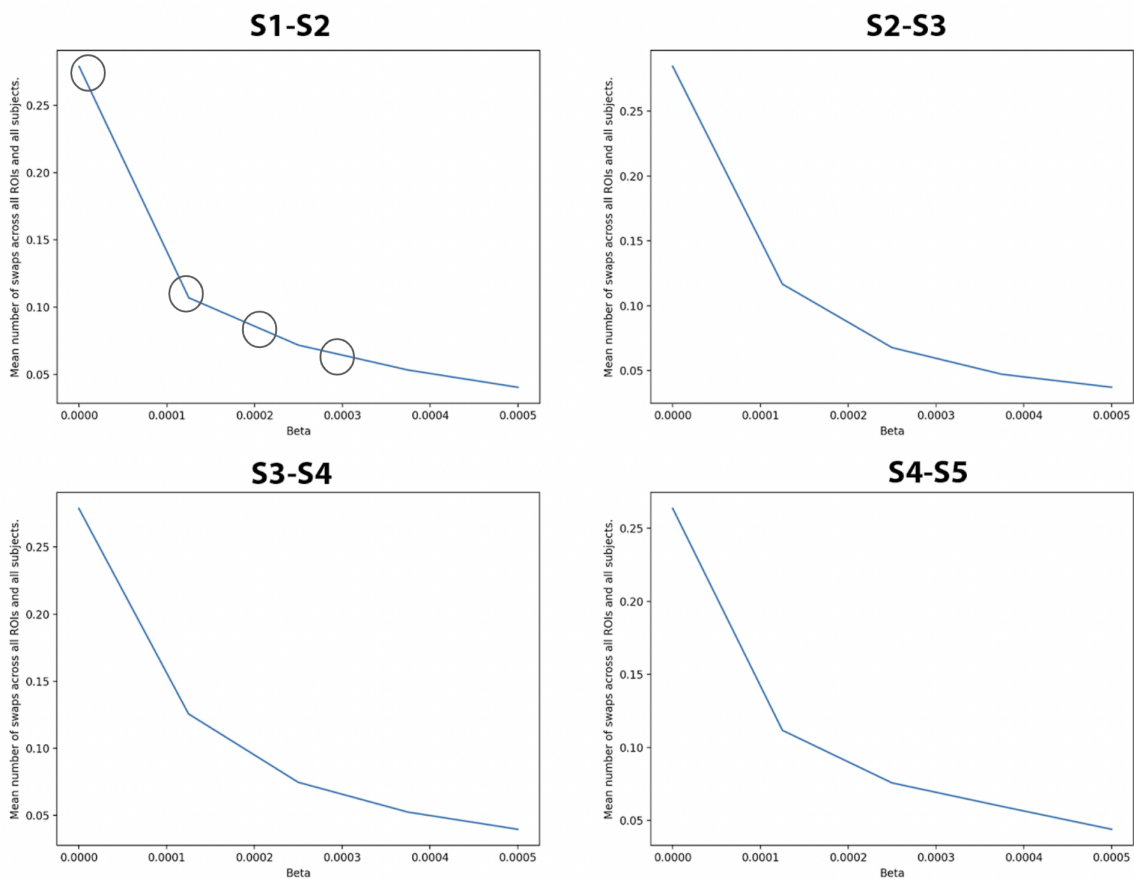


Figure S10: Proportion of swaps across all subjects and nodes with varying beta parameters. Circles in the top left figure indicate beta parameters chosen for subsequent analyses with varying β parameters.

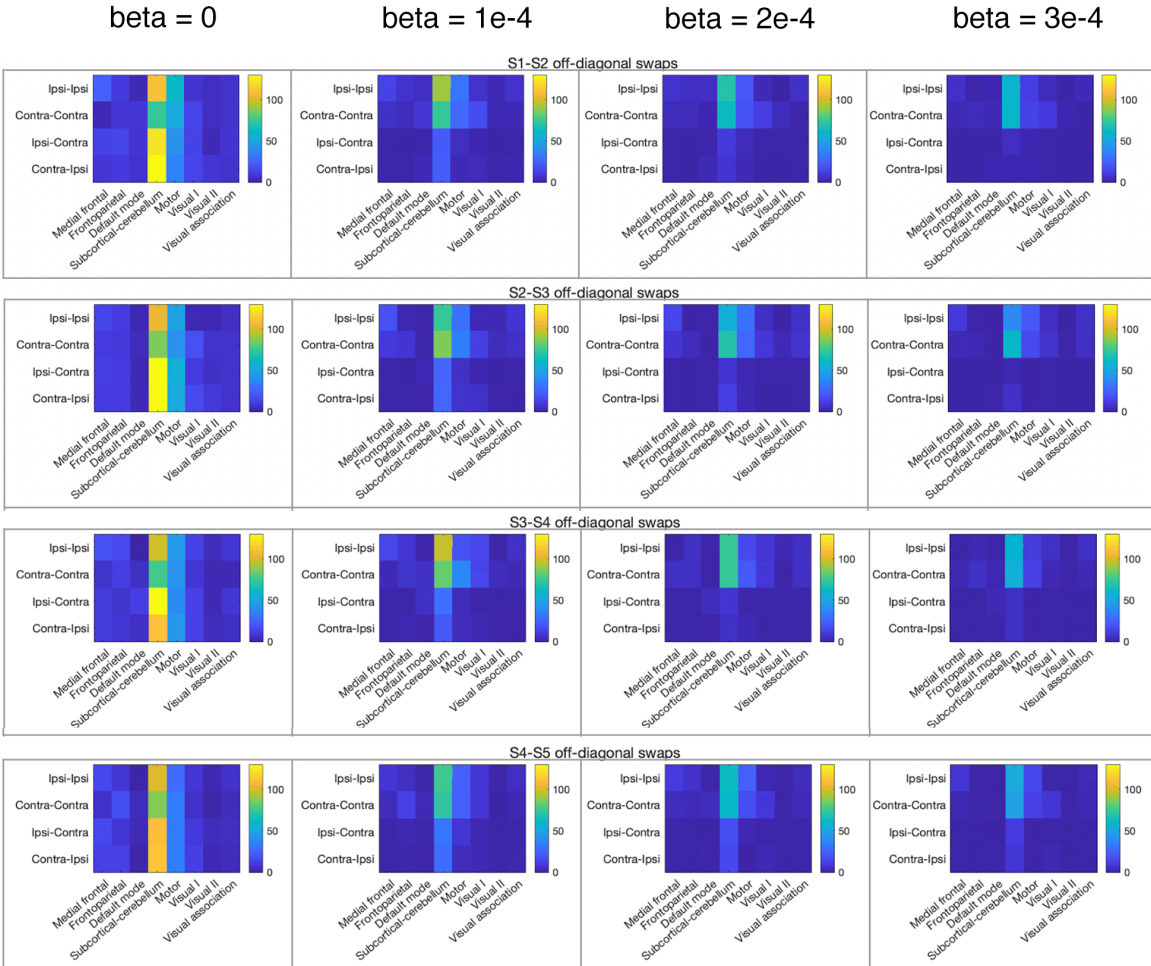


Figure S11: Impact of β on the sum of remaps within 8 functional networks, displayed separately depending on the source and target node's position relative to the lesion. (ipsilesional, same side as the lesion, and contralesional, opposite side as the lesion). Ipsi = ipsilesional, contra = contralesional. Ipsi-ipsi = ipsilesional node mapping to another ipsilesional node. Ipsi-contra = ipsilesional node mapping to a contralesional node. Contra-ipsi = contralesional node mapping to an ipsilesional node.

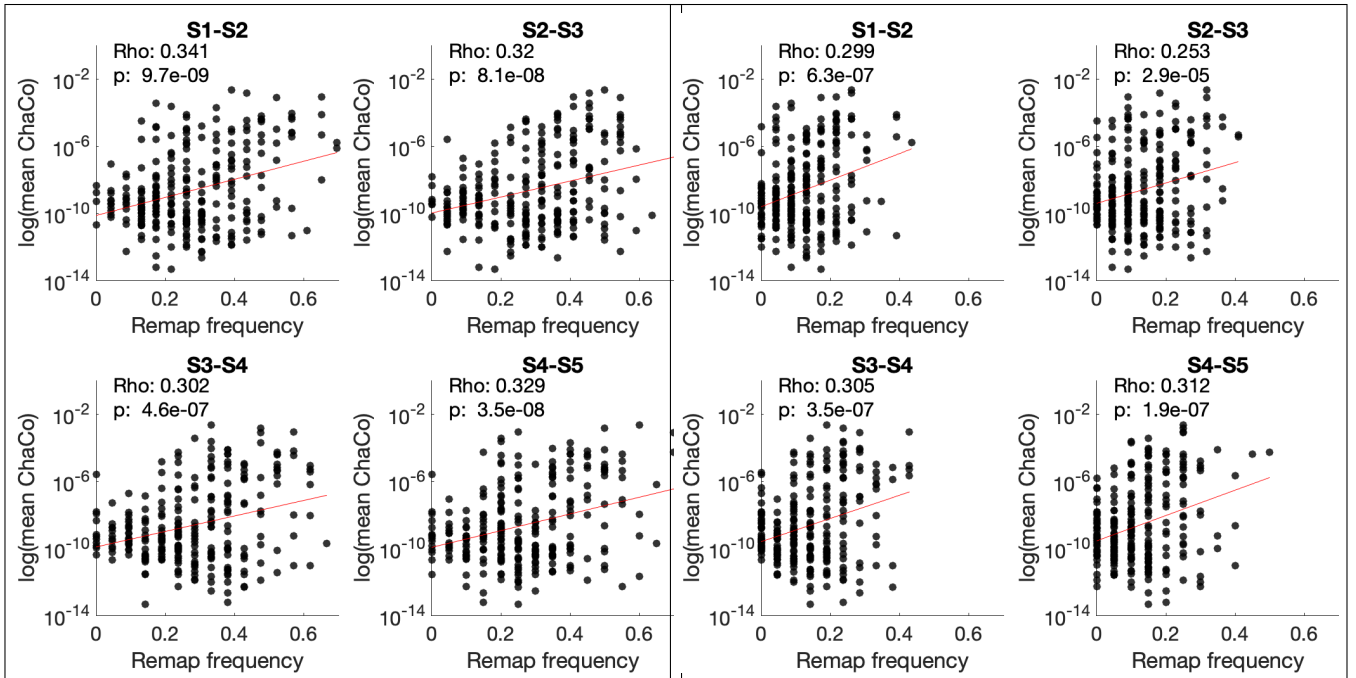
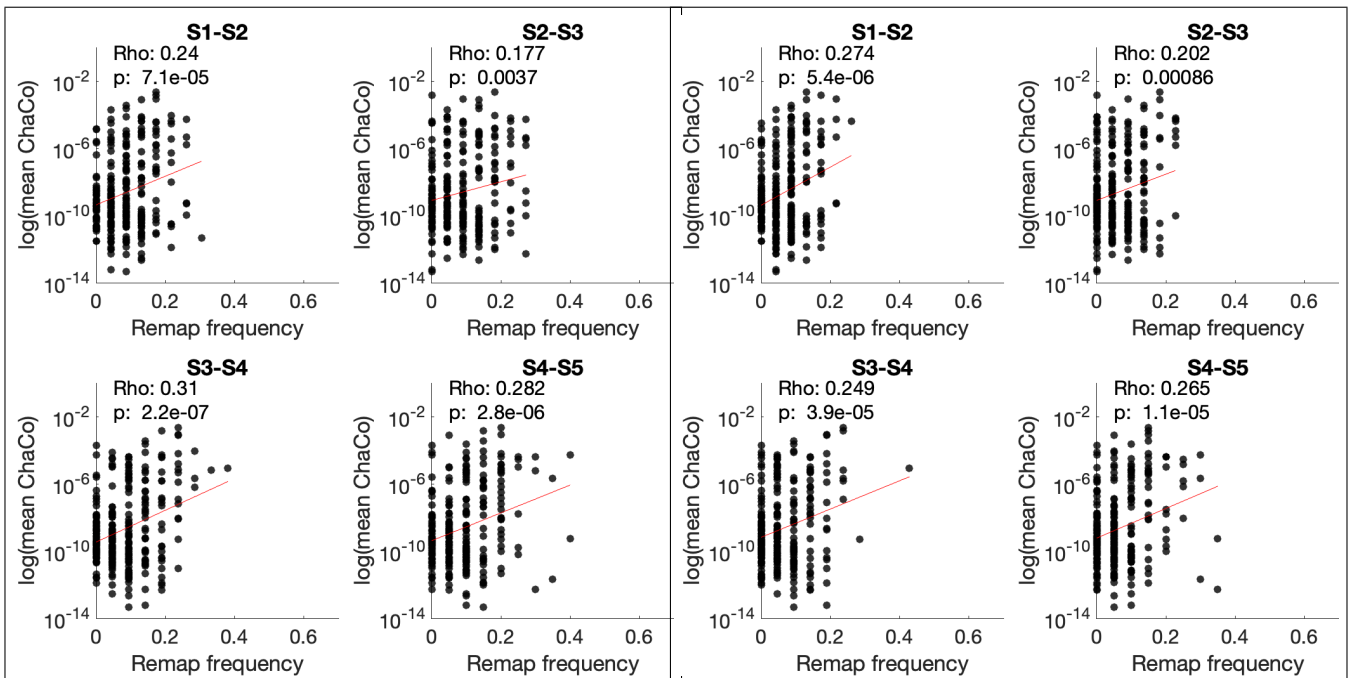
(a) Beta 1 ($\beta = 0$)(b) Beta 2 ($\beta = 1e-3$)(c) Beta 3 ($\beta = 2e-3$)(d) Beta 4 ($\beta = 3e-3$)

Figure S12: Varying betas - correlation between number of remaps and ChaCo scores

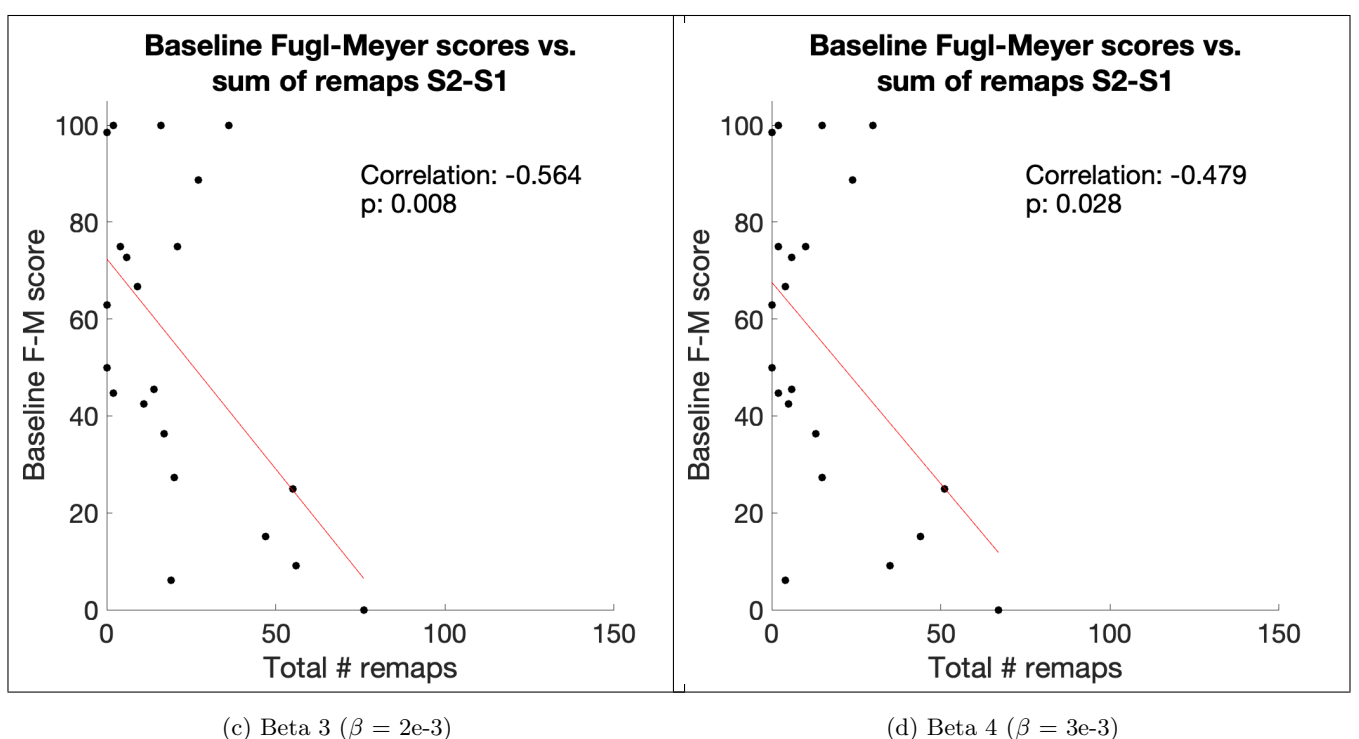
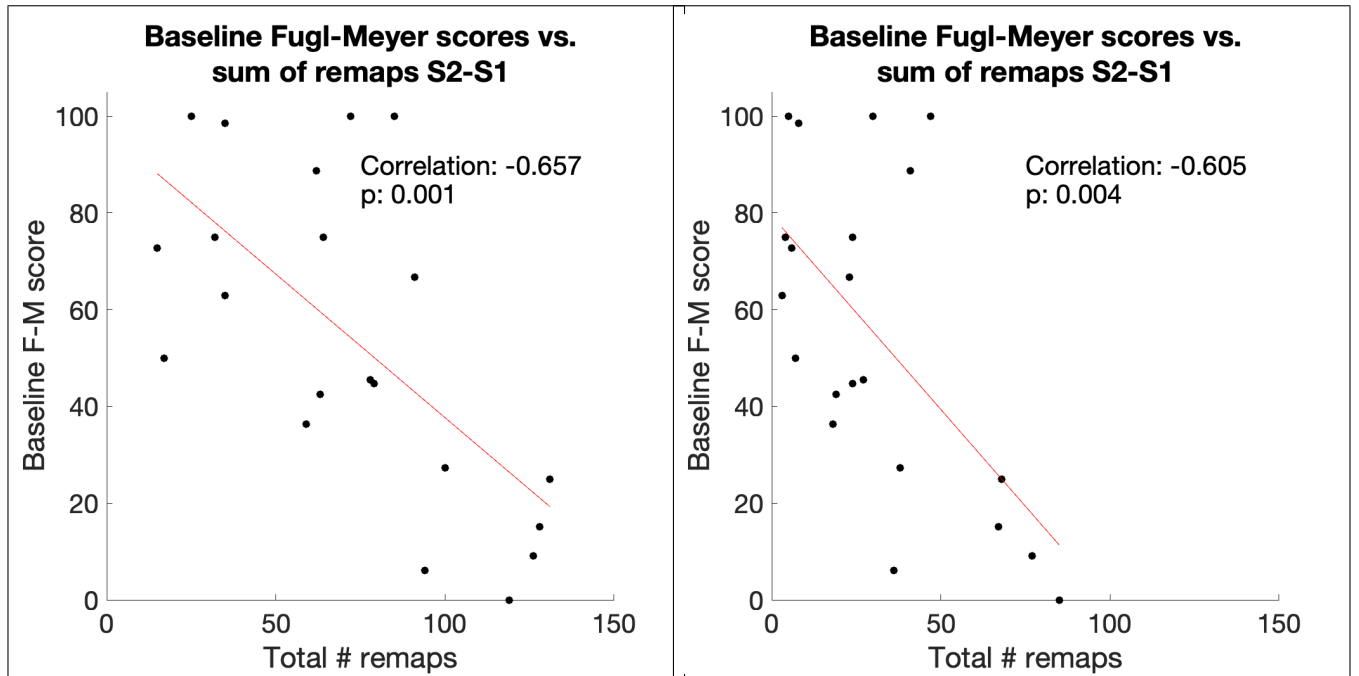
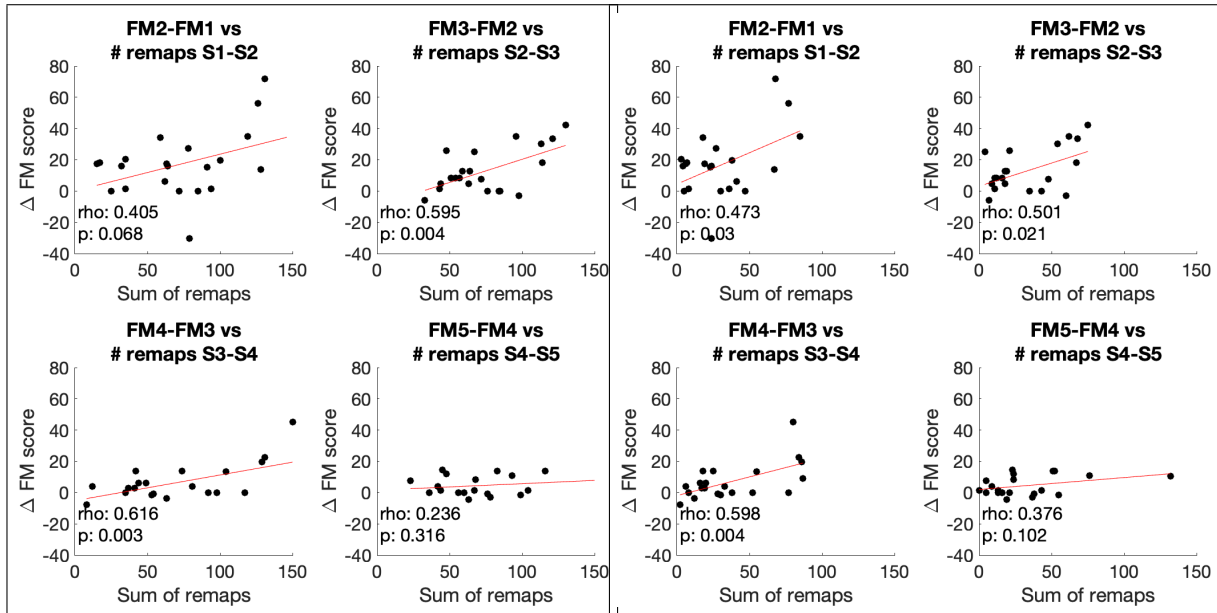
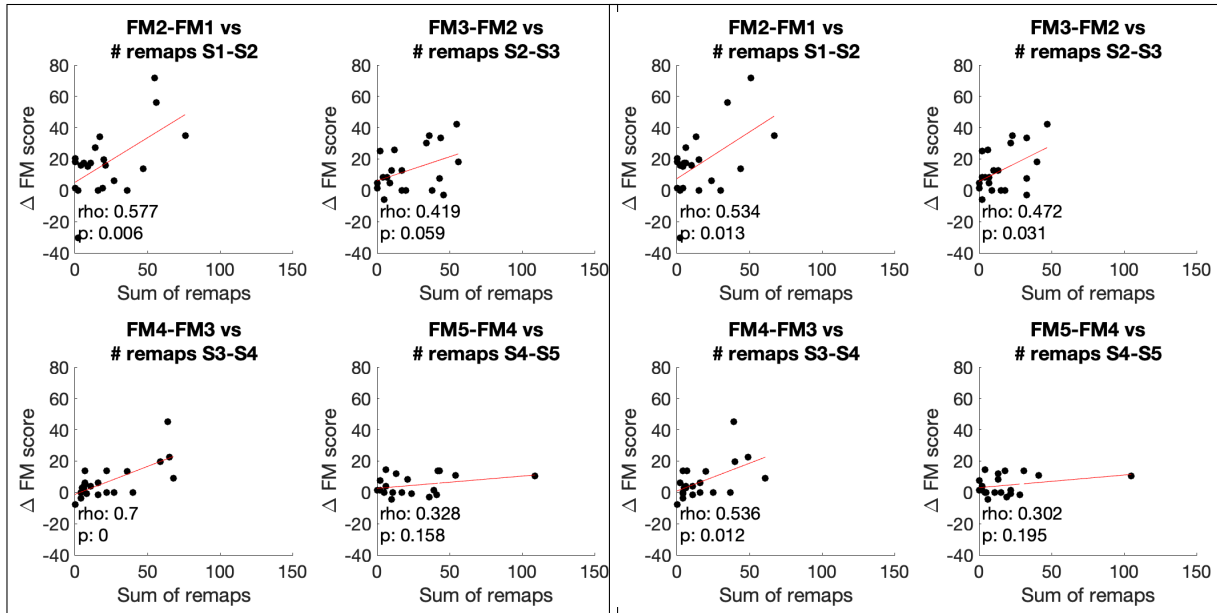


Figure S13: Varying beta does not change the significance of the relationship between total number of remaps between session 1 and session 2 and baseline Fugl-Meyer scores



(b) Beta 2 ($\beta = 1e-3$)



(d) Beta 4 ($\beta = 3e-3$)

Figure S14: Varying beta generally does not alter the relationships observed between session-specific increases in Fugl-Meyer scores and the number of remaps between sessions.

References

- [1] P W Duncan, S M Lai, and J Keighley. “Defining post-stroke recovery: implications for design and interpretation of drug trials”. en. In: *Neuropharmacology* 39.5 (Mar. 2000), pp. 835–841.
- [2] Maurizio Corbetta et al. “Neural basis and recovery of spatial attention deficits in spatial neglect”. en. In: *Nat. Neurosci.* 8.11 (Nov. 2005), pp. 1603–1610.
- [3] Ian R Winship and Timothy H Murphy. “Remapping the somatosensory cortex after stroke: insight from imaging the synapse to network”. en. In: *Neuroscientist* 15.5 (Oct. 2009), pp. 507–524.
- [4] Ramina Adam et al. “Functional reorganization during the recovery of contralateral target selection deficits after prefrontal cortex lesions in macaque monkeys”. en. In: *Neuroimage* 207 (Feb. 2020), p. 116339.
- [5] Yumi Murata et al. “Temporal plasticity involved in recovery from manual dexterity deficit after motor cortex lesion in macaque monkeys”. en. In: *J. Neurosci.* 35.1 (Jan. 2015), pp. 84–95.
- [6] Craig E Brown et al. “In vivo voltage-sensitive dye imaging in adult mice reveals that somatosensory maps lost to stroke are replaced over weeks by new structural and functional circuits with prolonged modes of activation within both the peri-infarct zone and distant sites”. en. In: *J. Neurosci.* 29.6 (Feb. 2009), pp. 1719–1734.
- [7] Alex R Carter et al. “Resting interhemispheric functional magnetic resonance imaging connectivity predicts performance after stroke”. en. In: *Ann. Neurol.* 67.3 (Mar. 2010), pp. 365–375.
- [8] M A Urbin et al. “Resting-state functional connectivity and its association with multiple domains of upper-extremity function in chronic stroke”. en. In: *Neurorehabil. Neural Repair* 28.8 (Oct. 2014), pp. 761–769.
- [9] Anne K Rehme and Christian Grefkes. “Cerebral network disorders after stroke: evidence from imaging-based connectivity analyses of active and resting brain states in humans”. en. In: *J. Physiol.* 591.1 (Jan. 2013), pp. 17–31.
- [10] Liang Wang et al. “Dynamic functional reorganization of the motor execution network after stroke”. en. In: *Brain* 133.Pt 4 (Apr. 2010), pp. 1224–1238.
- [11] Brenton Hordacre et al. “Fronto-parietal involvement in chronic stroke motor performance when corticospinal tract integrity is compromised”. en. In: *Neuroimage Clin* 29 (Jan. 2021), p. 102558.
- [12] Eva-Maria Pool et al. “Network dynamics engaged in the modulation of motor behavior in stroke patients”. en. In: *Hum. Brain Mapp.* 39.3 (Mar. 2018), pp. 1078–1092.
- [13] Jie Lu et al. “Focal pontine lesions provide evidence that intrinsic functional connectivity reflects polysynaptic anatomical pathways”. en. In: *J. Neurosci.* 31.42 (Oct. 2011), pp. 15065–15071.
- [14] V Saia and L Pantoni. “Progressive stroke in pontine infarction”. en. In: *Acta Neurol. Scand.* 120.4 (Oct. 2009), pp. 213–215.
- [15] Ying Wei et al. “Disrupted Regional Cerebral Blood Flow and Functional Connectivity in Pontine Infarction: A Longitudinal MRI Study”. en. In: *Front. Aging Neurosci.* 12 (Nov. 2020), p. 577899.
- [16] Caihong Wang et al. “Cerebral blood flow features in chronic subcortical stroke: Lesion location-dependent study”. en. In: *Brain Res.* 1706 (Mar. 2019), pp. 177–183.
- [17] G Liu et al. “Network change in the ipsilesional cerebellum is correlated with motor recovery following unilateral pontine infarction”. en. In: *Eur. J. Neurol.* 26.10 (Oct. 2019), pp. 1266–1273.
- [18] Emmanuel Carrera and Giulio Tononi. “Diaschisis: past, present, future”. en. In: *Brain* 137.Pt 9 (Sept. 2014), pp. 2408–2422.
- [19] Donatello Conte et al. “Thirty Years Of Graph Matching In Pattern Recognition”. In: *Int. J. Pattern Recognit Artif Intell.* 18.3 (May 2004), pp. 265–298.
- [20] Yusuf Osmanlıoğlu et al. “System-level matching of structural and functional connectomes in the human brain”. en. In: *Neuroimage* 199 (Oct. 2019), pp. 93–104.

- [21] X Shen et al. “Groupwise whole-brain parcellation from resting-state fMRI data for network node identification”. en. In: *Neuroimage* 82 (Nov. 2013), pp. 403–415.
- [22] Anirudh Wodeyar et al. “Damage to the structural connectome reflected in resting-state fMRI functional connectivity”. In: *Network Neuroscience* (July 2020), pp. 1–22.
- [23] Raphaël Liégeois et al. “Revisiting correlation-based functional connectivity and its relationship with structural connectivity”. In: *Network Neuroscience* (Aug. 2020), pp. 1–17.
- [24] A E Hillis et al. “Subcortical aphasia and neglect in acute stroke: the role of cortical hypoperfusion”. en. In: *Brain* 125.Pt 5 (May 2002), pp. 1094–1104.
- [25] Maurizio Corbetta et al. “Common behavioral clusters and subcortical anatomy in stroke”. en. In: *Neuron* 85.5 (Mar. 2015), pp. 927–941.
- [26] Amy Kuceyeski et al. “The Network Modification (NeMo) Tool: elucidating the effect of white matter integrity changes on cortical and subcortical structural connectivity”. en. In: *Brain Connect.* 3.5 (2013), pp. 451–463.
- [27] Emily S Finn et al. “Functional connectome fingerprinting: identifying individuals using patterns of brain connectivity”. en. In: *Nat. Neurosci.* 18.11 (Nov. 2015), pp. 1664–1671.